Lab on a Chip

PAPER

View Article Online
View Journal | View Issue

Cite this: *Lab Chip*, 2025, **25**, 3168

Late-stage placental barrier model for transport studies of prescription drugs during pregnancy†

Sonya Kouthouridis,[a] Poonam Saha,[b] Madeleine Ludlow,[c] Brenda Y. N. Truong[c] and Boyang Zhang *[ac]

Throughout pregnancy, the placental barrier is crucial for fetal development, evolving continuously to meet the growing nutritional demands of the fetus. Although the placenta has the capacity to selectively filter compounds, harmful xenobiotic substances from the maternal blood can sometimes cross over into the fetal circulation. This drives the development of *in vitro* placental barrier models in the context of drug transport studies. In this work, we adapted our lab's previous placental barrier model to transplacental drug transport by transitioning from self-assembled vasculature to a simplified straight tubular vasculature to improve throughput and consistency. We then closely examined the angiogenic cytokine secretion and crosstalk between trophoblasts and endothelial cells. Furthermore, we validated this model for drug barrier studies by assessing the permeability of three model therapeutic agents: paclitaxel, vancomycin, and IgG. Drug permeabilities were shown to be drug type, concentration, and size dependent, similar to what has previously been reported. The presented model offers a promising tool for enhancing drug safety assessments in pregnant women, ensuring both maternal well-being and fetal health.

Received 21st January 2025,
Accepted 22nd May 2025

DOI: 10.1039/d5lc00075k

rsc.li/loc

Introduction

Throughout pregnancy, the placental barrier continuously evolves to accommodate the nutritional demands of the developing fetus. At term, the placenta consists of branched chorionic villi which are bathed in a chamber of maternal blood and house the fetal vasculature (Fig. 1). A thin layer of fused syncytiotrophoblasts (STs) enclose these villi and a smaller population of undifferentiated cytotrophoblast cells (CTs), and various stromal cells are present between this syncytium and the endothelial layer constructing the fetal vasculature. Along with nutrients, waste and gases, drugs entering the maternal bloodstream can sometimes cross the placental barrier. Prescription drug use during pregnancy is often essential for maternal health and has steadily increased over the past three decades, particularly during the first trimester of gestation.[1] These medications range from antibiotics—comprising 80% of all prescriptions during pregnancy[2]—to psychotropics and chemotherapeutics. The most commonly prescribed psychotropics for anxiety and depression are selective serotonin reuptake inhibitors (SSRIs) and benzodiazepines (BZDs)[3] which have been shown to readily cross the placenta[4] and accumulate in fetal tissues.[5,6] In the instance of maternal infection, antibiotics may be prescribed to pregnant women, despite being shown to cross the placental barrier[7] and cause increased risks of asthma and changes in the fetal intestinal microbiome.[8] Alternatively, chemotherapy use during the first trimester is dangerous and can lead to the spontaneous termination of the pregnancy, therefore it is more likely to be prescribed during the 2nd and 3rd trimesters, when the risk of severe complications is reduced.[9] However, many studies evaluating the safety and side effects of these drugs are contradictory, which make it difficult to conclusively judge their safety.[10,11] Despite the potential negative side effects associated with these medications, it is crucial that pregnant women maintain access to them. The untreated ailments may pose greater risks than the listed side effects, therefore physicians must carefully weigh the necessity of treatment against the potential risks posed by the drugs. *In vitro* placental barrier models offer an ethical avenue to inform these decisions, facilitating the testing of drug treatment plans and the development of novel medications.

Many *in vitro* systems have been developed to mimic the placental barrier.[12] However, many of them have not successfully coupled a highly-differentiated ST layer with perfusable vasculature. In our previous work, we established a vascularized placental IFlowPlate model to simulate both

[a] *Department of Chemical Engineering, McMaster University, Hamilton, ON, L8S 4L8, Canada. E-mail: kouthous@mcmaster.ca, zhangb97@mcmaster.ca*
[b] *Michael G. DeGroote School of Medicine, McMaster University, Hamilton, ON, L8S 4L8, Canada. E-mail: poonam.saha@medportal.ca*
[c] *School of Biomedical Engineering, McMaster University, Hamilton, ON, L8S 4L8, Canada. E-mail: ludlowm@mcmaster.ca*

† Electronic supplementary information (ESI) available. See DOI: https://doi.org/10.1039/d5lc00075k

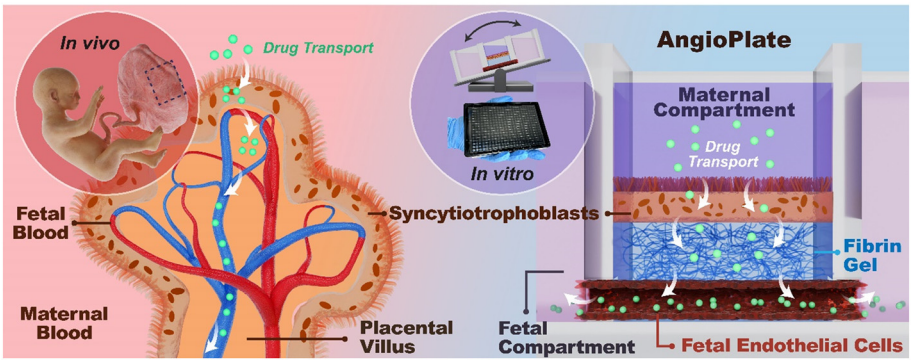

Fig. 1 Design of a single channel placental barrier model. Left. Placental chorionic villi consist of a thin multinucleated ST layer enclosing the fetal vasculature. Nutrients are transported from the maternal blood, through both the syncytial and endothelial barriers, to the fetal vasculature to meet the nutritional demands of the growing fetus. Right. The AngioPlate placental barrier model consists of a fibrin hydrogel acting as the interstitial space with a single vascular channel connecting it to the two adjacent wells. On the apical side of the gel, a ST monolayer is differentiated, and endothelial cells are seeded on the periphery of the vascular channel to form a vessel. The device is incubated on a tilting platform which permits media perfusion through the vessel. The single channel placental barrier model is designed based on a 384-well plate and can accommodate high-throughput studies.

early- and late-stage pregnancy which highlighted the importance of the vascular barrier in transplacental research.[13] This model exhibited impressive ST fusion rates, averaging 84.4 ± 1.0%, and featured self-assembled vasculature, enabling the development of intricate vascular networks that closely mimic physiological conditions. However, while these networks offer enhanced realism and permit the study of drugs on vasculogenesis, they pose challenges to reproducibility because of the unguided self-assembly of the cells. Further, lung fibroblasts were used in these tissues as they are commonly used to support vascular self-assembly. In addition, this model requires further validation to determine its effectiveness in drug transport studies.

To address some of these issues, we have streamlined our placental barrier model design by replacing the self-assembled vascular network with a single tubular blood vessel. This design change improved model consistency and experimental throughput as fewer cells are needed initially. In addition, without the need to optimize vascular self-assembly, there was greater freedom to use different types of vascular stromal cells. For our placenta models, placental pericytes were incorporated into the hydrogel matrix, in the place of conventional lung fibroblasts, to assess their capacity to support the vasculature of our model. Finally, this new model was used to assess the permeability of the commonly prescribed chemotherapeutic drug paclitaxel, the antibiotic vancomycin, and human immunoglobulin G (IgG) derived from human serum. The results demonstrated that placental permeability was dependent on both molecule size and concentration. Notably, fetal-to-maternal (F/M) concentration ratios were lowest for larger molecules, such as IgG and 65 kDa dextran, which crossed the placental barrier at significantly lower rates compared to smaller molecules like paclitaxel or vancomycin. Importantly, the model accurately reproduced the *ex vivo* permeability trends observed in placental explant perfusion studies for all three molecules.

Materials and methods

Cell culture

Placental stem cells (PSCs) (blastocyst-derived, RCB-4940, female) were procured from Riken BRC Cell Bank at passage number 17 and used until passage 23 in all experiments. Undifferentiated cells were maintained in expansion medium[14] consisting of DMEM/F12 + GlutaMAX supplemented with 2-mercaptoethanol (0.1×10^{-6} M), fetal bovine serum (FBS, 0.2%), penicillin–streptomycin (0.5%), bovine serum albumin (BSA, 0.3%), ITS (insulin, transferrin, selenium) media supplement (1%), L-ascorbic acid (1.5 μg mL^{-1}), EGF (50 ng mL^{-1}), CHIR99021 (2×10^{-6} M), A83–01 (0.5×10^{-6} M), SB431542 (1×10^{-6} M), VPA (0.8×10^{-3} M), and Y27632 (5×10^{-6} M). T75 flasks were precoated with a 10 μg ml^{-1} col IV solution in PBS and incubated for 1.5 hours at 37 °C. Cells were passaged when they reached 80% confluence by washing with PBS, then dissociating with TrypLE for 10–15 min and splitting at a 1 : 4 ratio onto collagen IV-coated flasks. Primary human umbilical vascular endothelial cells (HUVECs) were purchased from CedarLane Labs (CAP-0001GFP) and expanded in endothelial cell growth medium 2 (ECGM2, Sigma-Aldrich, C22011) supplemented with 1% antibiotic/antimycotic (100x, Sigma-Aldrich, A5955-100ML), on flasks coated with 0.2% gelatin, until passage 5. HUVEC/TERT2 cells were obtained from Evercyte (CHT-006-0008) and were expanded in ECGM2 supplemented with G418 (InvivoGen, ant-gn-1), an antibiotic acting as a selection agent to maintain the purity of the transfected culture. Both HUVEC types were dissociated with Trypsin-EDTA solution (0.05%) for 3 minutes at 37 °C and replated at a 1 : 4 ratio. Primary human placental pericytes (hPC-PL) were obtained from PromoCell (C-12980), cultured in pericyte growth medium 2 (PGM2, Millipore Sigma, C-28041) and used until passage 5. Pericytes were dissociated with StemPro™ Accutase™ (Thermofisher, A1110501) for 2–4 min at room temperature and replated at a 1 : 4 ratio according to the cell

bank's instructions. All cells were cultured at 37 °C with 5% CO_2.

AngioPlate manufacturing

The AngioPlate manufacturing protocol used in this work was adapted from the methods developed by Zhang *et al.*[15] Briefly, a 40% gelatin solution was prepared by dissolving gelatin from bovine skin (Sigma Aldrich, G9391) in water and autoclaving to dissolve and sterilize. Gelatin fibers were 3D printed onto pressure-adhesive sheets on a BIO X™ (Cellink) bioprinter with a 30G needle. The resulting gelatin channels had a diameter of 200 μm and were printed in a 384-well plate format. The patterned sheet was subsequently capped onto the base of a bottomless 384-well plate which had been milled with channels to accommodate the gelatin structures. Plates were UV sterilized for 10 minutes each side before use. These plates are also commercially available from OrganoBiotech (A002).

Establishment of model

A prepolymer fibrin gel solution was prepared by mixing 125 μL of 10 mg ml^{-1} fibrinogen (Sigma-Aldrich, F3879) with 25 μL of 10 U ml^{-1} thrombin (Sigma-Aldrich, T6884) in a 1.5 ml Eppendorf tube. 25 μL gels were immediately cast into the center wells of each AngioPlate device and allowed to crosslink at room temperature for 30 min. 90 μL of warmed PBS was added to each well and the plate was placed on a rocker (OrganoBiotech, B001) at 30 °C for 20 min to wash away the sacrificial gelatin channels. PBS was replaced and the plate was incubated in the same conditions for another 20 minutes. PBS was then aspirated and 50 μL of ECGM2 supplemented with 1% aprotinin was added to each center well and 90 μL into each adjacent well before placing the plate on the 37 °C rocker overnight. The next day, media was aspirated from all wells, being careful not to disturb the fibrin gel in the center compartments. A cell suspension of 500 000 HUVECs per ml was prepared and 120 μL was pipetted into both compartments adjacent to the gel. The hydrostatic pressure difference between the center and adjacent wells allows the cells to flow into the fibrin channel, which eventually becomes the vascular channel. Once seeded, the plate was incubated flat for 2 hours at 37 °C before 50 μL of media was added to the central gel. Media was changed daily by pipetting 50 μL into the center well and 80 μL into each adjacent well. On day 7 of culture, PSCs were added to the central compartment to form a monolayer of STs. Firstly, a 400 000 cell per ml suspension of PSCs was prepared in ST media[13,14] consisting of DMEM/F12 + GlutaMAX supplemented with 100 μM 2-mercaptoethanol, 0.5% penicillin–streptomycin, 0.3% BSA, 1% ITS media supplement, 25 μM Y27632, 2 μM forskolin, 4% KSR and 1% aprotinin. 60 μL of cell suspension were added to the central compartment and media was switched to a compartmentalized setup for the rest of the culture with ST media in the center and ECGM2 in the adjacent wells. Media was changed daily, and barrier analyses were performed after 8 days of coculture to allow for ST differentiation.

Incorporation of pericytes in model

Placental pericytes were incorporated into some models to determine whether they improve vascular barrier and/or placental barrier permeability. Before casting, the prepolymer fibrin gel solution was laden with pericytes at concentrations of either 50 000 cells per ml or 25 000 cells per ml. Gels were washed twice with PBS for 20 minutes, similar to the standard AngioPlate protocol above, however, 8% FBS was added to the ECGM2 media overnight to promote pericyte growth. Media was changed daily and HUVECs were added on day 2 of culture after which media was switched to ECGM2 without FBS. PSCs were added 7 days later, and cultures were maintained as described in the previous section. All media added to the platform included 1% aprotinin to control fibrin degradation over time.

Vascular permeability assay

A vascular permeability assay was performed before commencing coculture to confirm that the vasculature had formed correctly, and once again before every total barrier permeability assay to verify that vascular integrity was maintained during coculture. A solution of 1 mg ml^{-1} of TRITC-labelled 65 kDa dextran (Sigma-Aldrich, T1162) and 1 mg ml^{-1} of FITC-labelled 4 kDa dextran (Sigma-Aldrich, 46 944) was prepared in media. A standard curve was prepared by serially diluting the dextran solution (1 : 1, 1 : 10, 1 : 100, 1 : 1000 and 0 mg ml^{-1}) and pipetting 90 μL into each of three standard replicates. All media was aspirated from the plate, and 65 μL of fresh media was added to the center gel. Next, 90 μL of dextran solution was added to both adjacent wells to normalize the hydrostatic head in all three interconnect wells (90 μL dextran, 65 μL media + 25 μL gel, 90 μL dextran). Fluorescent measurements were immediately acquired with a Cytation5 plate reader and acquired again after placing the plate on the rocker for 1 h to determine vascular permeability under realistic culture conditions. When performing this assay in coculture, dextran solutions, as well as standard curves were prepared in 50/50 mixtures of the media used in the compartmentalized cultures. All data presented in the same plots were acquired on the same day.

Total permeability assay

Total dextran permeability of the AngioPlate placental barrier model was assessed by measuring the amount of dextran that diffused from the maternal compartment (central well above the STs) through the ST and endothelial layers, into the fetal compartments (adjacent wells). 4 kDa and 65 kDa fluorescently labeled dextrans were added into the maternal compartment at a 1 : 1 molar ratio (12.34 μg ml^{-1} and 200 μg ml^{-1}, respectively) in mixed media consisting of isovolumetric amounts of ECGM2 and STM. At t = 0 of this assay, media

was aspirated from all wells and 100 μL of 1 : 1 ECGM2 and STM was added to the fetal wells. 75 μL of the dextran solution was added to the central maternal compartment of the device to equilibrate media levels between compartments and avoid flow (25 μL gel + 75 μL dextran = 100 μL in center well). The plate was placed on a rocker at 37 °C for 24 hours, at which point fluorescence was analyzed to determine the amount of dextran permeated through the barrier model. Standard curves were prepared in a 1 : 1 media ratio of ECGM2 : STM to determine the final dextran concentrations in the fetal compartments. Fluorescent measurements were acquired using the Cytation5 plate reader. The absence of bleed-through between channels was confirmed in previous work.[13]

Immunostaining

AngioPlate gels were first washed with PBS for 5 min and then fixed with a 4% paraformaldehyde solution overnight in a 4 °C fridge, where all overnight immunostaining steps were performed. The next day, gels were washed with PBS three times for 10 min each and then fresh PBS was added overnight to remove any residual fixative. Cells were blocked and permeabilized overnight with a 10% FBS (Thermo Fisher Scientific, 12484028) and 0.1% Triton-X100 (Sigma-Aldrich) in PBS solution. Next, a primary antibody solution was prepared consisting of either anti-e-cadherin (1 : 200 dilution, Invitrogen, 13–1700), anti-ve-cadherin (1 : 1000, abcam, ab33168), anti-MRP1/P-gp (1 : 250, Enzo Life Sciences, ALX-801-007), anti-MDR1 (1 : 50, Santa Cruz Biotechnologies, sc-55 510) or anti-hCG (1 : 100, Sigma-Aldrich, SAB4500168) diluted in 2% FBS. Samples were incubated in the primary antibody solution overnight and washed thrice with PBS for 10 min. A secondary antibody solution consisting of anti-mouse FITC (1 : 1000 dilution, Sigma-Aldrich, F0257) or anti-rabbit CF594 (1 : 200, Sigma-Aldrich, SAB4600107-250UL), anti-rat Alexa 488 (1 : 500, Thermofisher, A11006) or anti-mouse CF 594 (1 : 200, Sigma-Aldrich, SAB4600105) and DAPI (1 : 1000, Sigma-Aldrich, D9542) in 2% FBS was applied to the gels overnight. The next day, tissues were washed in PBS thrice for 10 min, before being washed with fresh PBS overnight again. Samples were manually removed from the plate and imaged in a chamber slide *via* confocal microscopy (3i Marianas Lightsheet microscope).

Fusion percent quantification

Fusion analysis was performed on confocal images of tissues stained for DAPI and e-cadherin. Total cell number was determined by counting DAPI-stained nuclei in ImageJ. The e-cadherin stain was superimposed onto the DAPI image, and the fusion percent was determined by counting nuclei present in groups of at least three within a single e-cadherin boundary. The fusion percent was reported as the ratio between the number of fused nuclei and the number of total nuclei in each image.

Drug permeability assay

The drug permeability assay was designed in a similar way to the dextran permeability assay, where fluorescently labeled versions of the drugs were introduced into the central maternal compartment of the placental model and incubated for 24 h, then fluorescent readings of the adjacent fetal compartments were taken to determine drug concentrations. Paclitaxel (Oregon Green Conjugate, Sigma Aldrich, P22310) solutions were prepared at concentrations of 5 μM, 500 nM, and 50 nM in the 1 : 1 ECGM2 : STM mixed media. Vancomycin (FITC Conjugate, Sigma Aldrich, SBR00028) solutions were also prepared at concentrations of 5 μg ml^{-1}, 500 ng ml^{-1}, and 50 ng ml^{-1} in the 1 : 1 ECGM2 : STM mixed media. Finally, an IgG solution (FITC conjugate, Sigma Aldrich, F9636) of 1 mg ml^{-1} was prepared in the same media. At t = 0 of this assay, media was aspirated from all wells and 100 μL of 1 : 1 ECGM2 and STM was added to the fetal wells (left and right). 75 μL of one of the drug solutions was added to the central maternal compartment of the device. The plate was placed on a rocker at 37 °C for 24 hours and 70 μL of media was sampled from the fetal wells and pipetted into a black-walled and clear bottomed 384-well plate for fluorescence analysis. Standard curves for each one of these drugs were prepared in a 1 : 1 media ratio of ECGM2 : STM to determine the final drug concentrations in the fetal compartments. Fluorescent measurements were acquired using the Cytation7 plate reader at the excitation/emission wavelengths specified by the drugs' manufacturer.

Angiogenic cytokine analysis

AngioPlate tissues were cultured for 15 days with daily media changes to allow for ST differentiation. 24 hours after the last media change, supernatant from the central (apical) compartment and media from the adjacent (basolateral) compartments were collected. Supernatant was centrifuged at 1000 *g* for 10 minutes to precipitate any cell debris, and 70 μL of each sample was collected from the top surface of the vial. Samples were stored in −80 °C until they were sent to Eve Technologies for cytokine analysis. Samples were analyzed using the Human Angiogenesis & Growth Factor 17-Plex Discovery Assay® (HDAGP17) for the following biomarkers: Angiopoietin-2, BMP-9, EGF, Endoglin, Endothelin-1, FGF-1, FGF-2, Follistatin, G-CSF, HB-EGF, HGF, IL-8, Leptin, PLGF, VEGF-A, VEGF-C, VEGF-D. Secretion values under the detectable limit of the assay were presented as OOR (out of range).

Statistical analysis

All plots were generated and all statistics were performed using either paired t-test or one-way ANOVAs with Sidak's multiple comparison test in the GraphPad Prism software with 95% confidence (α = 0.05, $p < 0.05$). Normality was tested using the Shapiro–Wilk test and equal variance was tested using F-test. Data in all graphs were plotted as means with standard deviation shown as error bars.

Results

Model design

The late-stage placental barrier is primarily composed of a thin ST layer jacketing the chorionic villi, and an underlying endothelial layer that encloses the fetal blood (Fig. 1). A defining feature of this stage is the presence of a fully developed, perfusable, and permeability-selective vascular network representing the fetal circulation. In our model, we have incorporated both the mature ST layer and this functional vascular component to more accurately recapitulate the structure and function of the late-stage placental barrier. When designing this placental barrier model for drug safety studies, we applied a similar approach to our previous model[13] where a ST barrier, a fibrin gel matrix and a vascular barrier separate the fetal and maternal compartments of the model (Fig. 1). The stem cells used to form the ST layer of our placental barrier were derived using the protocol established by Okae *et al.*[14] In this study, we refer to these cells as placental stem cells (PSCs) to reflect their specific use in building placental tissue; however, they are functionally equivalent to the trophoblast stem cells (TSCs) described in the original Okae study. Further, the plate design is inspired by standard 384-well plates, enabling device compatibility with traditional imaging infrastructure and liquid handling tools. Wells are also connected in triplets (Fig. 1) to allow for perfusion of media throughout the vascular channel when incubating the plate on a tilting device.

To accommodate the requirements of high-throughput drug safety studies, we transitioned from the self-assembled vascular networks in the IFlowPlate platform to a straight, uniform vascular channel in our placental AngioPlate device (Fig. 1). The barrier's surface area plays a significant role in dictating both the rate and quantity of molecule permeation across a cell layer. Thus, ensuring consistency in barrier surface area across tissues is crucial for reliable comparisons of drug permeability data. This transition from self-assembled to straight vasculature not only increased tissue consistency but also eliminated the need for extensive optimization of culture conditions, resulting in a higher yield of perfusable tissues. Additionally, it improved model experimental throughput by reducing the initial cell requirements and offered greater flexibility in using various vascular stromal cell types. For instance, in some of our placenta models, placental pericytes were incorporated into the hydrogel matrix as a replacement for lung fibroblasts from previous work to assess their capacity to support vascularization.

To establish the model, we started with an AngioPlate with a sacrificial fiber patterned at the bottom of the well plate. Then a fibrin hydrogel was cast and crosslinked in the center well of the unit and the sacrificial template was dissolved away, resulting in a channel embedded in the hydrogel at the base of the central well. A ST layer was cultured on the surface of the gel, separating the gel from the central maternal compartment, whereas the fetal compartment consisted of the adjacent wells, connected by the endothelial-lined vascular channel (Fig. 1). Vascular stromal cells were embedded inside the fibrin gel surrounding the vascular channel as needed.

The effects of endothelial coculture on vascular barrier permeability

Establishing coculture models, especially with stem cells, can be challenging due to the unpredictable effects the media supplements of one cell type can have on the other. Further, cells release cytokines and other soluble factors that may affect the coculture's capacity to grow harmoniously. It is therefore imperative that coculture effects, as well as media effects, are evaluated in this placental barrier model. To do this, we assessed the permeability of AngioPlate cultures consisting of human umbilical vascular endothelial cells (HUVECs in ECGM2 media) cocultured with placental stem cells (PSCs) either in their undifferentiated CT-like state or after being differentiated into STs or extravillous cytotrophoblasts (EVTs) (Fig. 2A). Fluorescently labeled 4 kDa and 65 kDa dextrans were perfused through the vascular channel for one hour on day 15 of culture and fluorescent readings were taken (Fig. 2B, D and E). As anticipated, these cocultures resulted in confluent placental monolayers by day 15 with high fusion rates of 98.2 ± 0.2% and hCG secretion (Fig. 2C). The hCG expression observed in the ST monolayer is consistent with previous results from our IFlowPlate model,[13] which employed the same cell types under comparable experimental conditions, and whose extent of differentiation was validated *via* histology, fusion assay and gene expression analysis. To further confirm the specificity of hCG expression to differentiated STs, we performed immunostaining in a non-differentiated control group and observed significantly lower hCG signal intensity, supporting the differentiation-dependent nature of hCG expression in our model (ESI† Fig. S3). This outcome aligns with their intrinsic epithelial characteristics, reflecting their functional roles at distinct stages of gestation within the placental barrier. When comparing coculture to the HUVEC only condition, the diffusion of both 4 kDa and 65 kDa dextrans was highest in the PSCs + HUVECs conditions (1013.0 ± 120.9 pmol h^{-1} and 31.0 ± 4.6 pmol h^{-1}, respectively), suggesting that either PSC expansion media was incompatible with HUVEC culture or that undifferentiated PSCs release factors that break down the endothelial barrier (Fig. 2B, D and E). This could be due to the high media concentrations of valproic acid, a known HDAC inhibitor.[16] It has been shown that HDAC inhibition can lead to endothelial dysfunction,[17,18] whereas HDAC activation has been shown to drive CT fusion.[19] *In vivo*, undifferentiated CTs are most numerous and proliferative in the early stages of pregnancy, indicating HDAC inactivation, whereas vascular formation and syncytial fusion occur concurrently between the 4th and 10th weeks of gestation, indicating HDAC activation.

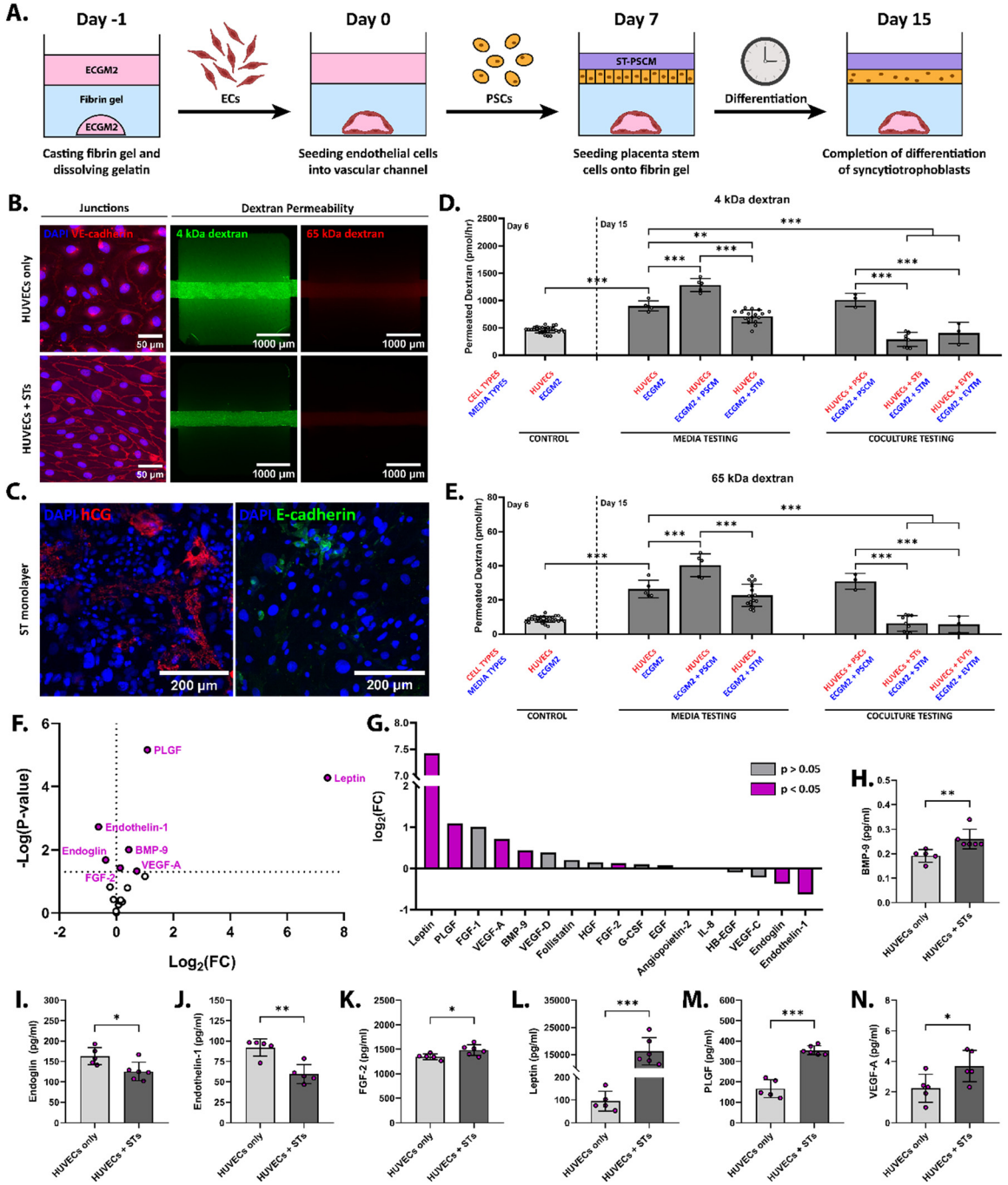

Fig. 2 The effects of ST coculture on endothelial barrier integrity and cytokine secretion. A. Timeline for placental barrier model establishment. On day −1, the fibrin hydrogel is cast, and the gelatin is allowed to dissolve with multiple PBS washes. On day 0, endothelial cells are seeded into the vascular channel and allowed to reach confluence before PSCs are added on day 7 and media is switched to compartmentalized culture. PSCs are differentiated into STs until day 15 when a dextran permeability analysis is usually performed. B. Immunostaining of endothelial junction marker VE-cadherin (red) and nucleic acids (DAPI, blue) in vascular tissues when cultured with and without differentiated STs. Fluorescent images of 4 kDa (green) and 65 kDa (red) dextran permeation through endothelial channel after 1 hour of perfusion. C. hCG (red) and e-cadherin (green) immunostaining of ST monolayer in HUVECs + ST coculture condition. D. Vascular permeability values on days 6 and 15 for FITC-labelled 4 kDa dextran after 1 hour of hydrostatic pressure-based vascular perfusion (two-way ANOVA, $*p < 0.05$, $**p < 0.01$, $***p < 0.001$). Media types and coculture conditions were tested. Datapoints from 3 separate experiments were combined in this plot. E. Vascular permeability values on days 6 and 15 for TRITC-labeled 65 kDa dextran after 1 hour of hydrostatic pressure-based vascular perfusion ($N = 3$, two-way ANOVA, $*p < 0.05$, $**p < 0.01$, $***p < 0.001$). Media types and coculture conditions were tested. Datapoints from 3 separate experiments were combined in this plot. F. *P*-value as a function of fold change in angiogenic cytokine secretion. Fold change is calculated as the secretion in the HUVECs + STs condition divided by that of the HUVECs only condition. G. Fold change in angiogenic cytokine secretion when adding STs to vascular culture. Cytokines are ordered from highest to lowest fold change. Bars colored in magenta exhibit significant differences in angiogenic cytokine secretion between HUVECs only and HUVECs + STs conditions. H–N. Angiogenic cytokine secretion of HUVECs only and HUVECs + ST barrier models 24 h after media change. ($N = 5$–6, two-tailed *t*-test, $*p < 0.05$, $**p < 0.01$, $***p < 0.001$).

Surprisingly, HUVECs exhibited the second-weakest barrier permeability (901.4 ± 91.8 pmol 4 kDa dextran per h and 26.4 ± 5.1 pmol 65 kDa dextran per h) despite being cultured alone in their specialized medium (ECGM2), which has been proven to maintain their morphology up until the 10th passage.[20] We hypothesize that this is due to the absence of stromal cells, which have been shown to support vascular formation and long-term stability in tissue engineered models.[21–24] ST + HUVEC cocultures seemed to have improved barrier permeability of both 4 kDa (289.8 ± 128.0 pmol h^{-1}) and 65 kDa dextran (6.3 ± 4.6 pmol h^{-1}) when compared to the HUVEC only control, with the ST + HUVEC condition being the least permeable. The HUVEC + EVT condition had statistically similar permeabilities (406.5 ± 195.6 pmol h^{-1} for 4 kDa dextran and 5.7 ± 4.8 pmol h^{-1} for 65 kDa dextran). Once again, these permeability results parallel the PIBF1 secretion profiles presented by Lee *et al.*, which showed that PSCs secreted the least amount of PIBF1 when compared to STs and EVTs.[25] This is reasonable given that, in early-stage pregnancy, when CTs are present in large quantities, blood vessels have not yet been formed. However, in the second and third trimesters when STs make up a larger proportion of trophoblasts within the placenta, perfusable fetal vasculature has been established. These results suggest that ST culture media may be supporting and strengthening the vascular barrier, or these cell types may be secreting factors that benefit the long-term culture of endothelial cells. A similar experiment was performed using immortalized TERT-HUVECs and similar trends were observed (Fig. S2†).

The effects of endothelial coculture on angiogenic cytokine secretions

To explain the differences in vascular barrier integrity between HUVEC only and HUVEC + STs conditions, cell culture supernatant was sampled from each culture and analyzed for the secretion of angiogenic cytokines: angiopoietin-2, BMP-9, EGF, endoglin, endothelin-1, FGF-1, FGF-2, follistatin, G-CSF, HB-EGF, HGF, IL-8, leptin, PLGF, VEGF-A, VEGF-C and VEGF-D (Fig. 2H–N, Fig. S1†). Although supernatant concentrations of angiopoietin-2, EGF, FGF-1, follistatin, G-CSF, HB-EGF, HGF, IL-8, VEG-C and VEG-D were statistically similar between these two culture conditions (Fig. 2F and G), we observed notable differences in 7 different cytokine profiles.

BMP-9 (bone morphogenetic protein 9) is a multifunctional protein and a member of the TGF-β family, whose main function consists of promoting bone and cartilage formation.[26] BMP-9 supernatant concentrations increased from 0.2 ± 0.03 to 0.3 ± 0.04 pg ml^{-1}, a 1.4-fold change (Fig. 2F–H), with the addition of STs to the culture. While trophoblasts contribute to placental development and vascularization, BMP-9 secretion by trophoblasts is not as well-documented or as prominent as its secretion by endothelial cells. STs may promote the production of BMP-9 in HUVECs to enhance angiogenesis and blood vessel formation, which is essential in pregnancy to support the growing fetus. Regardless, it has been shown that BMP-9 induces endothelial proliferation,[27] which suggests that it may play a role in increasing the confluence of the vascular culture, as seen from the vascular permeability assays (Fig. 2D and E). A smaller 1.1-fold increase was observed for FGF-2, whose concentrations went from 1.4 ± 0.1 to 1.5 ± 0.1 ng ml^{-1} with the addition of the trophoblast cells, suggesting that STs might also be stimulating FGF-2 secretion in endothelial cells (Fig. 2F, G and K). FGF-2 is a fibroblast growth factor known for its potent ability to stimulate the proliferation and differentiation of various cell types,[28] as well as its role in tissue repair and regeneration.[29] However, FGF-2 has also been shown to have angiogenic properties.[30] Cao *et al.* showed that, when micropellets containing FGF-2 were implanted into the corneas of mice, they induced a high density of blood vessels with very few fenestrations and low permeability, demonstrated *via* a ferritin permeability assay.[30] Therefore, similar to BMP-9, increased levels of FGF-2 in the media may be better maintaining the integrity of the vascular channel over long culture times.

Most drastically, leptin concentrations increased 171.2-fold when transitioning from the HUVEC monoculture to the HUVEC and ST coculture (Fig. 2F, G and L). Outside of pregnancy, this hormone's main function in the human body is to regulate hunger and metabolic rates.[31] However, during pregnancy, it plays a role in fetal development, nutrient transport, and angiogenesis.[32] This steep increase in supernatant concentrations of leptin is unsurprising, given that it has been well-documented that placental trophoblasts secrete leptin[33] to modulate embryo implantation, placental proliferation, as well as to further signal the metabolic demands and growth requirements of the developing fetus. However, leptin has been shown to activate angiogenesis[34] and to exert a protective effect on endothelial function,[35] which may explain why vascular integrity was maintained longer when HUVECs were cocultured with STs (Fig. 2B, D and E). The cytokine with the second-highest fold increase is placental growth factor (PLGF), a member of the vascular endothelial growth factor (VEGF) family of proteins, with concentrations of 166.1 ± 44.1 pg ml^{-1} for the HUVEC only condition and 354.2 ± 21.9 pg ml^{-1} for HUVEC and ST coculture (2.1-fold increase, Fig. 2F, G and M). PLGF is closely associated with placental development and has been known to enhance non-branching angiogenesis.[36] In fact, it has been reported that PLGF is primarily secreted by both EVTs and villous cytotrophoblasts,[36,37] however, it is also secreted by endothelial cells.[37] Although present in smaller concentrations, we see a similar trend in VEGF-A profiles when introducing STs to the HUVEC culture (2.2 ± 0.9 to 3.4 ± 1.0 pg ml^{-1}, 1.7-fold change, Fig. 2F, G and N), which can be explained by the fact that VEGF-A and PLGF are part of the same family of VEGFs, both being key drivers in angiogenesis.

Interestingly, levels of both endoglin and endothelin-1 were higher in the HUVEC only condition (162.8 ± 21.2 and 92.0 ± 10.7 pg ml^{-1}, respectively), when compared to the corresponding coculture condition (125.4 ± 22.7 and 59.6 ± 11.8 pg ml^{-1}, respectively, Fig. 2F, G, I and J). Endoglin is a co-receptor for TGF-β and is involved in angiogenesis and endothelial cell function. Lower levels of endoglin in the co-culture might reflect a feedback mechanism where STs downregulate endoglin to modulate the angiogenic response, possibly to prevent excessive or inappropriate vascular growth. Endothelin-1 is a potent vasoconstrictor that also has roles in inflammation and vascular remodeling. The reduced endothelin-1 in the coculture could suggest that STs suppress its production to maintain a more relaxed vascular environment, which would be beneficial for ensuring adequate blood flow to the developing placenta.

The increased levels of angiogenic factors (BMP-9, FGF-2, leptin, PLGF, and VEGF-A) support the formation of new blood vessels, which is essential in pregnancy. In contrast, the decreased levels of endoglin and endothelin-1 may reflect a controlled environment to prevent excessive vasoconstriction and to fine-tune the angiogenic process, ensuring a balanced and functional placental vasculature. Differences in the angiogenic cytokine profiles of these cultures suggest significant interactions between these two cell types that influence their behavior and the secretion of specific signaling molecules. The STs appear to influence HUVECs by modulating the secretion of cytokines and growth factors that are critical for angiogenesis and placental development.

The effects of media types on vascular barrier permeability

To decouple the effects of coculture and media type on vascular permeability, we next evaluated the permeability of the vascular channel cultured under different media conditions: ECGM2 only, compartmentalized media with PSCM in the center and ECGM2 in the adjacent compartments (ECGM2 + PSCM), and compartmentalized media with STM in the center and ECGM2 in the adjacent compartments (ECGM2 + STM). All three conditions were maintained exclusively in ECGM2 until day 6, mimicking the setup for coculture. On day 7, the mixed conditions were transitioned to compartmentalized media. As a result, the HUVECs cultured in ECGM2 on day 6 serve as the pre-compartmentalization control for all conditions. Dextran vascular permeability assays were performed both on day 6 and day 15 (Fig. 2D and E). Day 6 permeabilities to 4 kDa dextran ranged from 352.8 pmol h^{-1} to 567.4 pmol h^{-1} across all vascular tissues, and permeabilities to 65 kDa dextran ranged from 4.5 pmol h^{-1} to 12.6 pmol h^{-1} (Fig. 2D and E). Notably, vascular permeability in the HUVEC-only condition increased significantly from day 6 to day 15, indicating progressive barrier degradation over time. This functional decline is consistent with previous reports that VE-cadherin expression and endothelial integrity decrease in long-term HUVEC monocultures.[38] Therefore, the low VE-cadherin expression observed in Fig. 2B for the HUVEC-only group is expected and supports the importance of co-culture or media supplementation in maintaining barrier function. By day 15, dextran permeability was highest in the ECGM2 + PSCM condition (1285.9 ± 119.0 pmol 4 kDa dextran per h and 40.3 ± 6.7 pmol 65 kDa dextran per h), similar to what was observed in the coculture study with PSCs, suggesting that PSCM media alone can cause vascular disfunction (Fig. 2D and E). Interestingly, the ECGM2 + STM condition exhibited an increase in permeability from the day 6 control when assessed at day 15 of culture (713.0 ± 116.7 pmol 4 kDa dextran per h and 22.8 ± 6.5 pmol 65 kDa dextran per h), however not as much of an increase as was seen with the ECGM2 only condition (901.4 ± 91.8 pmol 4 kDa dextran per h and 26.4 ± 5.09 pmol 65 kDa dextran per h). As a result, between the three media conditions tested, culture of HUVECs in compartmentalized ECGM2 + STM conditions resulted in the lowest barrier degradation over time. This can possibly be explained by the presence of ROCK inhibitor Y27632 and cAMP activator forskolin in STM media, which have been shown to have protective effects on endothelial barrier permeability.[39–41] Notably, forskolin is also recognized for its capacity to promote the differentiation of stem cells into endothelial-like cells, emphasizing the critical role of the cAMP signaling pathway in endothelial cell culture.[42] In summary, media alone did not improve vessel function over time, this improvement is attributed to HUVEC coculture with STs, which may be secreting soluble factors that fortify the endothelial barrier. However, the ECGM2 + STM media configuration resulted in the least vascular barrier degradation over time.

Effects of pericytes on vascular barrier permeability

To study the effects of pericytes on feto-maternal transport, placenta-derived pericytes were introduced into our AngioPlate placental barrier system. *In vivo*, fetal pericytes provide support to the endothelial barrier, play a role in immune cell regulation and vascular development, and control blood flow through vessels.[43,44] However, their function in the placenta has not yet been heavily researched. Further, it has yet to be shown that they can be beneficial to the vascular barrier when incorporated into *in vitro* placental vascular models.[45] Given that none of these previous models included STs in their coculture designs[45,46] and that we showed that ST media and ST coculture help support the vascular barrier, we incorporated primary human placental pericytes (hPC-PL) as single-cell suspensions into the fibrin gel of our AngioPlate coculture with the goal of studying their effects on the model. Our AngioPlate system allows us to perform two types of barrier testing:[1] vascular barrier permeability, which measures the passage of fluorescently labeled particles through the HUVEC layer into the interstitial fibrin matrix during coculture and[2] total barrier permeability, which assesses the transport of particles across

both the HUVEC and ST layers into the fetal compartments. Both these assays are performed during coculture, which allows us to determine individual cell layer permeability whilst maintaining cellular crosstalk, which is not possible with conventional Transwell systems. To evaluate vascular permeability, 4 kDa and 65 kDa dextran were added to the inlet and outlet wells of the model and allowed to diffuse across the vascular barrier under perfusion conditions for 1 hour (Fig. 3A–C). The change in fluorescence intensity within the central fibrin compartment between $t = 0$ and $t = 1$ hour was used to quantify the amount of fluorescent dextran that permeated the vascular channel. A "no cell" control was included to demonstrate the unobstructed maximum diffusion through the fibrin gel, as well as a "ST only" control which would allow the isolation of the ST monolayer's influence on the placental barrier.

Although there was no significant difference in 65 kDa dextran diffusion in the no cell and the ST only conditions due to the absence of an endothelial barrier in both (56.1 ± 5.2 pmol h^{-1} and 56.1 ± 5.3 pmol h^{-1}, respectively, Fig. 3C), the smaller 4 kDa dextran showed marginally decreased diffusion through the STs only condition (1268 ± 132 pmol h^{-1}) when compared to the no cell control (1457 ± 74 pmol h^{-1}, Fig. 3B). This could be explained by the fact that the ST cells create a barrier between the media in the gel and the media above the ST cells, which can reduce the volume into which the 4 kDa dextran diffused. The presence of a ST monolayer therefore resulted in a different concentration gradient throughout the gel, which is the driving factor in

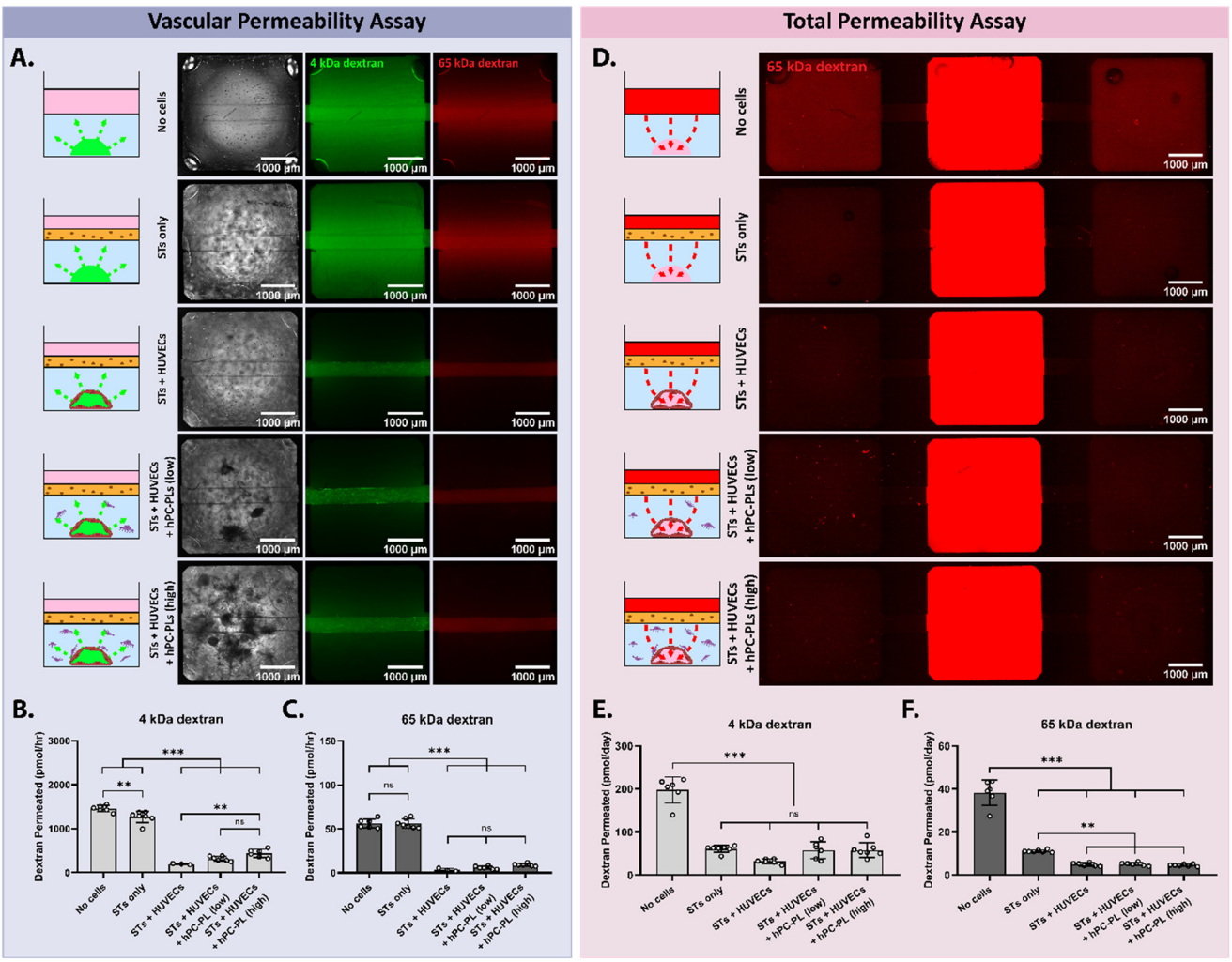

Fig. 3 Effects of pericytes on vascular and total permeability of placental barrier model on days 16 and 18 of culture. A. Brightfield images of vascular channel for the following conditions: no cell control, ST only, ST + HUVECs, and two tricultures with ST + HUVECs + hPC-PLs at high and low density. Fluorescent images of 4 kDa (green) and 65 kDa (red) dextran permeation through the endothelial channel after 1 hour of perfusion. B. Vascular barrier permeability to 4 kDa dextran. (N = 3–7, one-way ANOVA, *$p < 0.05$, **$p < 0.01$, ***$p < 0.001$) C. Vascular barrier permeability to 65 kDa dextran. (N = 3–7, one-way ANOVA, *$p < 0.05$, **$p < 0.01$, ***$p < 0.001$) D. Fluorescent images of 65 kDa dextran (red) permeating from the central maternal compartment, through the ST and HUVEC barriers, to the adjacent fetal compartments after 24 hours. E. Total barrier permeability to 4 kDa dextran from the maternal to the fetal compartments. (N = 6–7, one-way ANOVA, **$p < 0.01$, ***$p < 0.001$) F. Total barrier permeability to 65 kDa dextran from the maternal to the fetal compartments. (N = 6–7, one-way ANOVA, ***$p < 0.001$).

diffusion. As expected, 65 kDa dextran diffusion was much lower in all three vascularized conditions (3.4 ± 1.7 pmol h^{-1} for STs + HUVECs, 9.0 ± 1.5 pmol h^{-1} for STs + HUVECs + hPC-PL (high) and 5.8 ± 1.7 pmol h^{-1} for STs + HUVECs + hPC-PL (low)), however the addition of pericytes did not have any effect on vascular permeability of this larger dextran.

In the case of 4 kDa dextran, the vascularized conditions once again exhibited lower permeabilities (195.9 ± 14.7 pmol h^{-1} for STs + HUVECs, 440.4 ± 92.9 pmol h^{-1} for STs + HUVECs + hPC-PL (high) and 317.4 ± 54.5 pmol h^{-1} for STs + HUVECs + hPC-PL (low)). Interestingly, the addition of a higher density of pericytes increased the permeability of the vascular channel to 4 kDa dextran when compared to the ST + HUVEC condition. However, because this increase was small and was not paralleled in the 65 kDa dextran experiment, it is implied that the changes in transplacental permeability were minimal. To investigate the specific contribution of pericytes to vascular integrity independently of ST influence, we performed an additional experiment in which pericytes were cocultured with GFP-HUVECs alone. In this setup, we observed that pericytes enhanced vascular barrier integrity, supporting their known role in stabilizing and supporting microvasculature (Fig. S4†).

The increased permeability observed in the ST + HUVEC + hPC-PL (high) condition may be attributed to pericyte-induced matrix degradation or excessive cell proliferation, potentially leading to nutrient and oxygen depletion within the culture. This overgrowth may have been driven by the presence of PSC media supplements or by interactions with the STs. Thus, further optimization of culture conditions is needed to support the inclusion of a third cell type in this model. Alternatively, the lack of an observed barrier-enhancing effect from pericytes may reflect a ceiling effect, wherein the STs already provided maximal support to the vasculature, leaving little room for further improvement.

Effects of pericytes on total barrier permeability

Once vascular permeability was assessed, the permeability of the entire placental barrier was evaluated (Fig. 3D–F). As expected, the no cell control exhibited the highest permeation of both dextran types (197.5 ± 30.2 pmol per day for 4 kDa and 38.3 ± 5.9 pmol per day for 65 kDa dextran) and the three vascularized tissues exhibited the lowest 65 kDa dextran permeability (4.9 ± 0.8 pmol per day for ST + HUVECs, 4.5 ± 0.5 pmol per day for ST + HUVECs + hPC-PL (high) and 5.0 ± 0.8 pmol per day for ST + HUVECs + hPC-PL (low)) and no significant differences among them (Fig. 3E and F), similar to the vascular permeability assay (Fig. 3B and C). The ST only condition's permeability was significantly higher (11.0 ± 0.6 pmol per day) which could be explained by there being one cell barrier for the dextran to permeate through as opposed to the two in the vascularized models. Interestingly, there was no difference between 4 kDa dextran permeabilities in all four cell conditions. However, the ST+HUVEC condition (31.8 ± 5.7 pmol per day) trended toward being significantly different from the ST only condition (60.5 ± 8.0 pmol per day) and the two conditions containing pericytes (57.8 ± 17.0 pmol per day for high density and 57.5 ± 19.8 pmol per day for low density, respectively). Considering that the pericytes offered no improvement in vascular or total barrier permeability and that their overgrowth in the culture resulted in the overtaking of the vascular channel in some tissues and likely caused a reduction of nutrient availability for the endothelial and trophoblast cells, pericytes were not included in any future placental AngioPlate cultures.

Drug barrier study

To assess the suitability of our platform for drug transport studies, we determined the permeability of our barrier system to three therapeutic agents: paclitaxel, a chemotherapeutic drug that triggers mitotic arrest and apoptosis in cancer cells,[47] vancomycin, an antibiotic primarily prescribed to treat Gram-positive bacterial infections,[48] and immunoglobulin G from human serum, which is used in a variety of therapeutic strategies for patients with primary antibody deficiencies.[49,50] These drugs were selected because of their known transport profiles supported by *in vivo* data and because they span the range of small molecules to large proteins. Fluorescently labeled versions of these drugs were introduced into the central maternal compartment of the device and incubated for 24 hours with vascular perfusion, before fetal concentrations were analyzed *via* fluorescent intensity measurement. A similar assay was also performed with fluorescently labeled dextrans (4 kDa and 65 kDa) to isolate the effects of molecular size on permeability.

Breast cancer is the most common cancer type diagnosed during pregnancy, accounting for 40% of all cancer diagnoses, followed by lymphoma (12%) and cervical cancer (10%).[51] Paclitaxel and other taxane therapies have been shown to be a viable option for women suffering from cancer during pregnancy.[52–54] Paclitaxel concentrations of 5 μM, 500 nM and 50 nM were introduced into the central maternal compartment. As expected, paclitaxel permeation into the fetal compartment was proportional to paclitaxel concentrations in the maternal media. Values ranged from 10.1 ± 3.4 pmol per day for the 5 μM maternal values to 0.3 ± 0.1 pmol per day for 500 nM, and values were out of range (OOR) for 50 nM (Fig. 4A). This same downward trend was observed in the fetal-maternal (F/M) paclitaxel ratios (1.0 ± 0.3% for 5 μM, 0.3 ± 0.1% for 500 nM, OOR for 50 nM), suggesting diffusion-driven permeation that is dependent on concentration gradients (Fig. 4E). In comparison, Nekhayeva *et al.* perfused the maternal artery of 7 placental explants with 100 nM of paclitaxel for 2 hours and showed that the concentration of paclitaxel in the fetal circuit were also low at 4.3 ± 2.2%[55] (Fig. 4G). Similarly, a baboon study showed that fetal paclitaxel levels paralleled maternal concentrations at

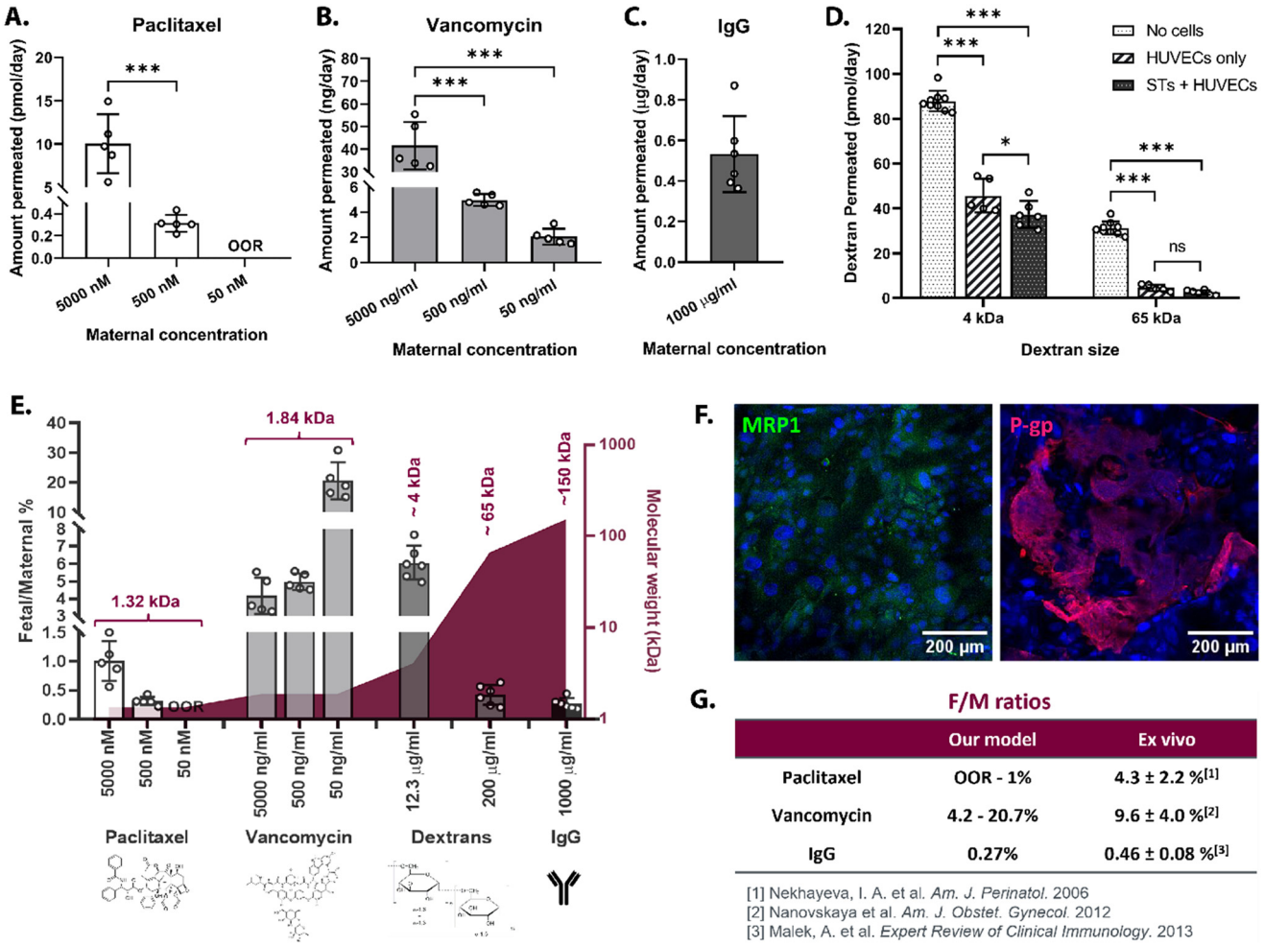

Fig. 4 Drug permeability of AngioPlate placental barrier model. A.–C. Permeation of paclitaxel, vancomycin and immunoglobulin G from the maternal compartment to the fetal compartment after 24 h of vascular perfusion. OOR: out of range. (N = 5, one-way ANOVA, $*p < 0.05$, $**p < 0.01$, $***p < 0.001$) D. Total barrier permeability to 4 kDa and 65 kDa dextrans from the maternal to the fetal compartments in no cell, HUVEC only and STs + HUVECs conditions. (N = 5, one-way ANOVA, $*p < 0.05$, $**p < 0.01$, $***p < 0.001$) E. Fetal to maternal (F/M) ratios of drugs and dextrans after 24 hours of vascular perfusion at different molecular concentrations. Secondary y-axis displays the molecular weight of the fluorescently labeled molecules. (N = 5–6) F. Immunofluorescent staining of drug transporters in the ST monolayer of the placental barrier model. MRP1 is shown in green and P-gp in red, highlighting their expression and localization within the syncytiotrophoblast layer. G. F/M ratios of *ex vivo* placental explants for paclitaxel,[55] vancomycin[57] and IgG[58] from human serum.

rates approximately 100 times lower and the drug was undetectable in the fetal tissues at necropsy.[56]

Vancomycin is an antibiotic drug commonly prescribed to treat serious bacterial infection during pregnancy. It has been confirmed to cross the placental barrier and to cause significant changes in the fetal microbiome and kidney injury in animal studies,[8,59] however has not been shown to cause adverse effects during human pregnancy.[2] Three vancomycin solutions were prepared at concentrations of 5 µg ml^{-1}, 500 ng ml^{-1} and 50 ng ml^{-1} and introduced into the maternal well. Similarly, vancomycin levels in the fetal compartment correlated to those in the maternal compartment with 41.6 ± 10.5 ng per day for a maternal concentration of 5 µg ml^{-1}, 5.0 ± 0.5 ng per day for 500 ng ml^{-1}, 2.1 ± 0.6 ng per day for 50 ng ml^{-1} (Fig. 4B). However, an inverse correlation between F/M values and maternal vancomycin concentrations was observed (4.2 ± 1.1% for 5 µg ml^{-1} of maternal vancomycin, 5.0 ± 0.5% for 500 ng ml^{-1}, 20.7 ± 6.2% for 50 ng ml^{-1}), suggesting that the transport of this antibiotic across the placental barrier may be transport-driven (Fig. 4E). Further, although vancomycin and paclitaxel have similar molecular weights, their transport rates and F/M ratios differ significantly. This indicates that drug transport is influenced, at least to some extent, by the trophoblast layer, rather than occurring solely through simple diffusion. The vancomycin F/M ratios obtained in this study are consistent with those reported in *ex vivo* placental perfusion experiments.[57,60] For instance, Nanovskaya *et al.* perfused placental explants with 25 µg mL^{-1} of vancomycin for 4 hours, observing a final F/M percentage of 9.6 ± 4% in the fetal circulation[57] (Fig. 4G). Interestingly, *in vivo* studies measuring cord blood vancomycin concentrations in pregnant women have shown

that fetal vancomycin levels can eventually reach maternal concentrations during maternal antibiotic infusions.[61–63] Notably, these *in vivo* permeability values are higher than those observed in *in vitro* or *ex vivo* barrier models.[60] It has been suggested that the presence of heparin in the media used for *in vitro* and *ex vivo* studies may lead to the formation of a heparin-vancomycin complex,[60] which reduces the transplacental passage of vancomycin. In the present study, heparin, present in ECGM2 at concentrations higher than those in maternal blood, may have contributed to the reduced passive diffusion of vancomycin across the placental model.

The permeability of immunoglobulin G (IgG) from human serum was assessed at a maternal concentration of 1 mg mL^{-1}, revealing a transport rate across the placental barrier of 0.5 ± 0.2 μg per day, corresponding to an F/M percentage of 0.3 ± 0.1% (Fig. 4C). As anticipated, the transfer of IgG into the fetal compartment was significantly lower compared to smaller molecules such as dextrans, paclitaxel, and vancomycin, primarily due to its larger size, which restricts passive diffusion. Beyond passive diffusion, IgG transport is facilitated by neonatal Fc receptors (FcRn) expressed on the ST surface, enabling selective antibody transport, with a preference hierarchy of IgG1 > IgG3 > IgG4 > IgG2.[64] Clements *et al.* conducted a meta-analysis of 17 studies measuring maternal and cord IgG levels at birth, demonstrating that F/M ratios can exceed 1.0 by term due to months of active antibody transport.[65] This contrasts with the lower F/M ratios observed in this study, which reflect only 24 hours of experimental conditions. In our previous work, we confirmed FcRn expression in STs through analysis of the FCGRT gene and found it to be comparable to levels in BeWo b30 cells,[13] which are known to possess functional FcRn receptors.[66] To further verify the presence of these receptors, future experiments could incorporate FcRn localization staining and inhibitor treatments to validate their role in antibody transport. In contrast, *ex vivo* placental perfusion studies have reported F/M IgG ratios comparable to those observed in our experiments (Fig. 4E and G). For instance, Malek *et al.* demonstrated that IgGs cross into the fetal compartment at approximately 0.5% of maternal concentrations after 6 hours of perfusion.[67] Similarly, Miller *et al.* observed a fetal concentration of 0.6 ± 0.3% of the maternal IgG1 antibody I-F105 following a 6-hour perfusion.[68] These findings reinforce the notion that IgG transfer across the placenta in *ex vivo* models is limited over short experimental time frames due to the highly selective and time-dependent nature of FcRn-mediated transport.

To assess the impact of size on barrier permeability and to elucidate the cumulative barrier effects of the ST and EC barriers, we employed 4 kDa and 65 kDa dextrans (Fig. 4D), which are considered relatively inert to mammalian cells,[69] in a similar fluorescence-based assay. Permeability to 65 kDa dextran was statistically similar for the single layer HUVECs only conditions (4.7 ± 1.4 pmol per day) and the double layer STs + HUVECs condition (2.6 ± 1.1 pmol per day), but much lower than the no cell control (31.2 ± 3.0 pmol per day). This suggests that the HUVEC barrier is so minimally permeable to 65 kDa that the extra ST layer has no discernible effect, which agrees with previous findings of HUVEC dextran permeability.[70] When converting the 65 kDa dextran permeability rate of the ST + HUVEC condition to a F/M ratio, we obtain a value of 0.4 ± 0.2%, which is higher but in the same order of magnitude as that of IgG (0.3 ± 0.1%, Fig. 4E). This can be explained by the fact that these molecules are of similar sizes, with IgGs averaging a higher molecular weight of 150 kDa.[71] In contrast, the smaller 4 kDa dextran permeated the STs + HUVECs barrier (37.3 ± 6.0 pmol per day) at a lower rate than the HUVEC only culture (45.6 ± 7.5 pmol per day), due to the fact that the endothelial layer is semi-permeable to smaller dextrans.[70] The fetal/maternal ratios of 4 kDa dextran in the ST + HUVEC coculture equate to 6.1 ± 1.0%, which is closer to that of smaller molecules such as vancomycin (4.2 ± 1.1% for 5 μg ml^{-1} of maternal vancomycin, 5.0 ± 0.5% for 500 ng ml^{-1}, 20.7 ± 6.2% for 50 ng ml^{-1}). In summary, these findings confirm that the permeability of our placental barrier model is molecule size, concentration, as well as drug-type dependent and can therefore be used to explore the safety of many commonly prescribed medications during pregnancy.

Discussion

The placenta serves as the primary site of exchange between the mother and fetus, making it a key focus of studies aimed at understanding which xenobiotic compounds can cross into the fetal circulation. In this work, we designed a scalable placental barrier model consisting of a ST layer separating the maternal compartment from the model fetal vessel. Primary CT cells have long been regarded as the gold standard for *in vitro* human placental cultures due to their genetic similarity to *in vivo* tissues. However, they present significant challenges, including limited accessibility, demanding maintenance requirements, and the potential for spontaneous differentiation. Trophoblast stem cells and the associated differentiation protocol used in this paper were established by Okae *et al.* and have achieved large-scale popularity in *in vitro* placental modeling due to their capacity to differentiate into a highly fused syncytium.[14] In our previous work, we compared the differentiation capacity of these stem cells to the model choriocarcinoma cell line BeWo b30 by evaluating their fusion percentage, hCG secretion rates, polarity, morphology and gene expression.[13] We determined that the stem cells were immensely better at differentiating into STs and they have since become the cell type of choice for our models.

In this current placental barrier model, we first evaluated the effects of ST coculture on the endothelial vasculature, as well as the effects of the corresponding mixed coculture medium. We found that the ST cells assumed a protective role for the endothelial culture by secreting pro-angiogenic factors that support vascular growth. Leptin and PLGF levels

in the device's media supernatant were drastically increased by 171.2- and 2.1-fold, respectively, with the addition of trophoblasts to the system. This coincided with an improvement in vascular channel integrity, decreased vessel leakiness and stronger staining of ve-cadherin. These findings align with previous studies investigating the roles of leptin and PLGF both *in vivo* and *ex vivo* endothelium. PlGF has been shown to strongly activate the ERK1/2 pathway in endothelial cells, which controls cell proliferation, angiogenesis, vascular permeability and response to hypoxic stress.[72,73] For example, Chau *et al.* showed that treatment with PlGF increased cell proliferation under hypoxic conditions for both trophoblast and endothelial cells.[74] Similarly, leptin has been shown to have strong angiogenic effects *in vivo* and *in vitro*.[75] Although the effects that these pro-angiogenic cytokines have on endothelial cells have been widely studied, this study is the first to investigate how the inclusion of trophoblasts influences vascular permeability to small molecules. In addition to driving the secretion of angiogenic cytokines ST layers reached confluence faster when cocultured with endothelial cells, suggesting a possible positive feedback loop between ST and endothelial cells.

Another key point in this study was to evaluate the effects of incorporating placental pericytes into the model on barrier effectiveness. Pericytes are known to direct branching angiogenesis and control blood flow rates in other human organs,[76] however, their function in the human placenta has not been extensively explored. Interestingly, pericytes preferentially cover endothelial junctions furthest away from the trophoblast layer,[77] suggesting that trophoblast-pericyte crosstalk modulates pericyte localization in the placenta. In this study, we demonstrated that the presence of pericytes in our placental barrier model did not enhance barrier integrity, which led to their exclusion from the final model. However, Haase *et al.* showed that the addition of placental pericytes was detrimental to their placental microvascular model because they triggered preeclampsia-associated cytokine production, inhibited vascular growth and caused microvascular leakage.[45] The authors attributed this to an imbalance in endothelial-pericyte communication, more specifically a disruption of signaling through the VEGF-Ang-Tie2 pathway, demonstrating the importance of the optimization of these types of cocultures.

In this work we quantified transport of three drugs across our placental barrier and compared the fetal/maternal permeation rates to those reported from *ex vivo* cultures. Fluorescently labelled paclitaxel, vancomycin, dextran and IgG were selected to span both the size and types of molecules that may be transported into the fetal bloodstream. These molecules traverse the placental barrier through various mechanisms, including passive diffusion, facilitated diffusion, active transport, exocytosis and endocytosis, and transporter proteins.[78] The transport profiles observed will typically reflect the specific transport mechanisms associated with each type of molecule.

Paclitaxel is often prescribed as a cancer treatment during pregnancy because it transfers to the fetus at concentrations below 5% of those found in maternal circulation. This limited transfer is primarily due to the efflux transporter P-glycoprotein (P-gp), which actively transports paclitaxel—and other substances such as antibiotics, steroids, and protease inhibitors—back into the maternal circulation from placental cells. Consequently, this mechanism effectively reduces fetal exposure to these compounds. In our previous work, we showed that our STs express P-gp at similar rates as BeWo b30, which are known to express these functional transporters.[79] In the current study, we further confirmed the presence of P-gp in the AngioPlate model by performing MDR1 immunostaining, as shown in Fig. 4F. We also stained for MRP1, another key efflux transporter involved in placental drug resistance and observed robust expression in the ST monolayer (Fig. 4F), further supporting the model's physiological relevance. Our permeability data (Fig. 4A and E) demonstrates that as paclitaxel concentrations in the maternal bloodstream increase, so too do the concentrations in the fetal bloodstream, highlighting this transport dynamic. A similar trend was observed with the fetal concentrations of vancomycin (Fig. 4B and E), which is of a similar size to paclitaxel and is primarily transported across the placenta *via* passive diffusion. When this data is converted to fetal/maternal ratios, we observed lower F/M ratios for paclitaxel, which can be explained by the presence of P-gp efflux transporters actively removing large concentrations of paclitaxel molecules from the placental cells. The dextrans, which are also transported across the placenta *via* passive diffusion, had fetal concentrations and F/M ratios reflective of their size. 4 kDa dextran had F/M ratios similar to those of vancomycin (Fig. 4E), which has a molecular weight of 1.84 kDa, whereas the 65 kDa dextran has much lower F/M ratios given the larger molecule size will cause steric hindrance during passive diffusion. IgGs, which have an average molecular weight of 150 kDa, crossed the placental barrier at even lower F/M rates, as expected. This new transporter characterization supports the relevance of our model for studying both passive and active mechanisms of drug transport across the placental barrier. When expanding the list of drugs tested on this model it could be beneficial to identify the localization of certain transporters to thus associate the quantity of drug permeation to the transport type.

The PSCs used in this work were first developed in 2018 by Okae *et al.* from blastocyst and CT-derived cells.[14] However, to create a large library of PSCs from patients with diverse genetic backgrounds, regular access to human embryos and first-trimester placentas would be required using this protocol. To address this, Castel *et al.* developed a cellular reprogramming protocol starting with adult human somatic or pluripotent cells and resulting in induced trophoblast stem cells akin to post-implantation day 8–10 CTs.[80] Using an adapted Okae differentiation protocol, these induced trophoblast stem cells were successfully

differentiated into both STs and EVTs, showcasing a promising approach for placental research with patient-derived cells.

Many placental organoid model systems have since been developed using this cell type or differentiation protocol.[80–85] In fact, this protocol has been applied to generate differentiated trophoblast organoids from both patient-derived somatic cells and induced pluripotent stem cells.[80–82] However, most post-culture analyses focused primarily on genetic sequencing and localized marker expression, with minimal inclusion of functional assays or detailed organoid characterization. Nonetheless, even the most complex placental organoid models suffer from incompatibility with permeability testing given the inaccessibility of their central compartment. In our AngioPlate placental model, not only can we perform barrier testing, but we have the ability to separately assess the permeability of the vascular channel or the syncytial barrier (vascular permeability assay *vs.* total permeability assay) during coculture, which is not possible using conventional Transwell systems. For total permeability analysis, this functional assay is highly scalable, facilitating high-throughput drug screening by quantifying permeated drugs *via* mass spectrometry—a method particularly advantageous when fluorescently-tagged drugs are limited in availability. Further, the composition of the model's fibrin hydrogel matrix is compatible with protein and RNA extraction methods, as shown in our previous work.[13] In fact, Carrion *et al.* showed that the fibrinolytic protease nattokinase has the capacity to cleave fibrin bonds within a cell-laden fibrin hydrogel to obtain a single-cell suspension.[86] The resulting samples can then be used for downstream applications of proteomics or gene sequencing. Given the important advantages of these systems, chip and plate-based models will remain the standard for *in vitro* placental transport studies.

Conclusion

High fidelity *in vitro* placental barrier models are necessary to determine the safety of prescription drug regimes during pregnancy. In this work, we engineered a 3D placental barrier model that incorporates both differentiated ST and endothelial layers and is compatible with the high-throughput requirements of drug safety assays. Once the coculture model was established, we showed that the ST cells and their media perform a supportive role in maintaining vascular barrier integrity over 18 days in culture, allowing for efficient syncytial differentiation of the trophoblasts, which is vital to term placental modeling. This extended culture time offers the opportunity for longer drug treatment studies in future work. Finally, when assessing the permeability of three drug types (chemotherapeutics, antibiotics, and antibodies) we determined that the barrier permeability was dependent on molecule size, type, and concentration, agreeing with *in vivo* and *ex vivo* literature findings.

Data availability

The datasets generated during the current study are available from the corresponding author upon reasonable request.

Author contributions

S. K. performed the experiments, analyzed the results, and prepared the manuscript. P. S. assisted with the design and manufacturing of AngioPlates. M. L. contributed to stem cell culture and immunostaining. B. Z. envisioned the concept, supervised the work and edited the manuscript.

Conflicts of interest

B. Z. holds equities in OrganoBiotech, Inc. which is commercializing the AngioPlate Platform used in this work.

Acknowledgements

This work was made possible by the financial support of the Natural Sciences and Engineering Research Council of Canada (NSERC) Discovery Grant (RGPIN-05500-2018) and Canadian Institute of Health Research (CIHR) Project Grant (PJT-166052) to B. Z. The authors gratefully acknowledge the use of BioRender (**https://www.biorender.com**) for the creation of the illustrations in this work. The authors would like to thank Justin Bernar from the Chemical Engineering Department Machine Shop at McMaster University for his help milling all the plates used in this work.

References

1 M. M. Werler, S. M. Kerr, E. C. Ailes, J. Reefhuis, S. M. Gilboa and M. L. Browne, *et al.*, Patterns of Prescription Medication Use during the First Trimester of Pregnancy in the United States, 1997–2018, *Clin. Pharmacol. Ther.*, 2023, **114**(4), 836–844.
2 P. B. Bookstaver, C. M. Bland, B. Griffin, K. R. Stover, L. S. Eiland and M. McLaughlin, A Review of Antibiotic Use in Pregnancy, *Pharmacotherapy*, 2015, **35**(11), 1052–1062.
3 C. E. Creeley and L. K. Denton, Use of Prescribed Psychotropics during Pregnancy: A Systematic Review of Pregnancy, Neonatal, and Childhood Outcomes, *Brain Sci.*, 2019, **9**(9), 235.
4 J. Rampono, K. Simmer, K. F. Ilett, L. P. Hackett, D. A. Doherty and R. Elliot, *et al.*, Placental Transfer of SSRI and SNRI Antidepressants and Effects on the Neonate, *Pharmacopsychiatry*, 2009, **42**(3), 95–100.
5 L. C. Meng, C. W. Lin, H. M. Chuang, L. K. Chen and F. Y. Hsiao, Benzodiazepine Use During Pregnancy and Risk of Miscarriage, *JAMA Psychiatry*, 2024, **81**(4), 366–373.
6 H. van Hove, L. Mathiesen, J. J. M. Freriksen, K. Vähäkangas, A. Colbers and P. Brownbill, *et al.*, Placental transfer and vascular effects of pharmaceutical drugs in the human placenta ex vivo: A review, *Placenta*, 2022, **122**, 29–45.

7 G. G. Nahum, K. Uhl and D. L. Kennedy, Antibiotic Use in Pregnancy and Lactation: What Is and Is Not Known About Teratogenic and Toxic Risks, *Obstet. Gynecol.*, 2006, **107**(5), 1120.
8 M. M. Alhasan, A. M. Cait, M. M. Heimesaat, M. Blaut, R. Klopfleisch and A. Wedel, *et al.*, Antibiotic use during pregnancy increases offspring asthma severity in a dose-dependent manner, *Allergy*, 2020, **75**(8), 1979–1990.
9 S. Esposito, R. Tenconi, V. Preti, E. Groppali and N. Principi, Chemotherapy against cancer during pregnancy, *Medicine*, 2016, **95**(38), e4899.
10 J. R. Daw, G. E. Hanley, D. L. Greyson and S. G. Morgan, Prescription drug use during pregnancy in developed countries: a systematic review, *Pharmacoepidemiol. Drug Saf.*, 2011, **20**(9), 895–902.
11 B. D. Wesley, C. A. Sewell, C. Y. Chang, K. P. Hatfield and C. P. Nguyen, Prescription medications for use in pregnancy–perspective from the US Food and Drug Administration, *Am. J. Obstet. Gynecol.*, 2021, **225**(1), 21–32.
12 M. Cherubini, S. Erickson and K. Haase, Modelling the Human Placental Interface In Vitro—A Review, *Micromachines*, 2021, **12**(8), 884.
13 S. Kouthouridis, A. Sotra, Z. Khan, J. Alvarado, S. Raha and B. Zhang, Modeling the Progression of Placental Transport from Early- to Late-Stage Pregnancy by Tuning Trophoblast Differentiation and Vascularization, *Adv. Healthcare Mater.*, 2023, **12**(32), 2301428.
14 H. Okae, H. Toh, T. Sato, H. Hiura, S. Takahashi and K. Shirane, *et al.*, Derivation of Human Trophoblast Stem Cells, *Cell Stem Cell*, 2018, **22**(1), 50–63.e6.
15 F. Zhang, D. S. Y. Lin, S. Rajasekar, A. Sotra and B. Zhang, Pump-Less Platform Enables Long-Term Recirculating Perfusion of 3D Printed Tubular Tissues, *Adv. Healthcare Mater.*, 2023, **12**(27), 2300423.
16 M. Göttlicher, S. Minucci, P. Zhu, O. H. Krämer, A. Schimpf and S. Giavara, *et al.*, Valproic acid defines a novel class of HDAC inhibitors inducing differentiation of transformed cells, *EMBO J.*, 2001, **20**(24), 6969–6978.
17 A. Zampetaki, L. Zeng, A. Margariti, Q. Xiao, H. Li and Z. Zhang, *et al.*, Histone Deacetylase 3 Is Critical in Endothelial Survival and Atherosclerosis Development in Response to Disturbed Flow, *Circulation*, 2010, **121**(1), 132–142.
18 T. Kashio, K. Shirakura, M. Kinoshita, M. Morita, R. Ishiba and K. Muraoka, *et al.*, HDAC inhibitor, MS-275, increases vascular permeability by suppressing Robo4 expression in endothelial cells, *Tissue Barriers*, 2021, **9**(3), 1911195.
19 G. J. Bhattad, M. J. Jeyarajah, M. G. McGill, V. Dumeaux, H. Okae and T. Arima, *et al.*, Histone deacetylase 1 and 2 drive differentiation and fusion of progenitor cells in human placental trophoblasts, *Cell Death Dis.*, 2020, **11**(5), 1–17.
20 K. Bala, K. Ambwani and N. K. Gohil, Effect of different mitogens and serum concentration on HUVEC morphology and characteristics: Implication on use of higher passage cells, *Tissue Cell*, 2011, **43**(4), 216–222.
21 E. A. Margolis, D. S. Cleveland, Y. P. Kong, J. A. Beamish, W. Y. Wang and B. M. Baker, *et al.*, Stromal Cell Identity Modulates Vascular Morphogenesis in a Microvasculature-on-a-Chip Platform, *Lab Chip*, 2021, **21**(6), 1150–1163.
22 S. Alimperti, T. Mirabella, V. Bajaj, W. Polacheck, D. M. Pirone and J. Duffield, *et al.*, Three-dimensional biomimetic vascular model reveals a RhoA, Rac1, and N-cadherin balance in mural cell–endothelial cell-regulated barrier function, *Proc. Natl. Acad. Sci. U. S. A.*, 2017, **114**(33), 8758–8763.
23 S. J. Grainger, B. Carrion, J. Ceccarelli and A. J. Putnam, Stromal Cell Identity Influences the In Vivo Functionality of Engineered Capillary Networks Formed by Co-delivery of Endothelial Cells and Stromal Cells, *Tissue Eng., Part A*, 2013, **19**(9–10), 1209–1222.
24 R. Costa-Almeida, M. Gomez-Lazaro, C. Ramalho, P. L. Granja, R. Soares and S. G. Guerreiro, Fibroblast-Endothelial Partners for Vascularization Strategies in Tissue Engineering, *Tissue Eng., Part A*, 2015, **21**(5–6), 1055–1065.
25 J. G. Lee, J. M. Yon, G. Kim, S. G. Lee, C. Y. Kim and S. A. Cheong, *et al.*, PIBF1 regulates trophoblast syncytialization and promotes cardiovascular development, *Nat. Commun.*, 2024, **15**(1), 1487.
26 T. Blunk, A. L. Sieminski, B. Appel, C. Croft, D. L. Courter and J. J. Chieh, *et al.*, Bone Morphogenetic Protein 9: A Potent Modulator of Cartilage Development In Vitro, *Growth Factors*, 2003, **21**(2), 71–77.
27 Y. Suzuki, N. Ohga, Y. Morishita, K. Hida, K. Miyazono and T. Watabe, BMP-9 induces proliferation of multiple types of endothelial cells in vitro and in vivo, *J. Cell Sci.*, 2010, **123**(10), 1684–1692.
28 L. A. Solchaga, K. Penick, J. D. Porter, V. M. Goldberg, A. I. Caplan and J. F. Welter, FGF-2 enhances the mitotic and chondrogenic potentials of human adult bone marrow-derived mesenchymal stem cells, *J. Cell. Physiol.*, 2005, **203**(2), 398–409.
29 D. S. Park, J. C. Park, J. S. Lee, T. W. Kim, K. J. Kim and B. J. Jung, *et al.*, Effect of FGF-2 on Collagen Tissue Regeneration by Human Vertebral Bone Marrow Stem Cells, *Stem Cells Dev.*, 2015, **24**(2), 228–243.
30 R. Cao, A. Eriksson, H. Kubo, K. Alitalo, Y. Cao and J. Thyberg, Comparative Evaluation of FGF-2–, VEGF-A–, and VEGF-C–Induced Angiogenesis, Lymphangiogenesis, Vascular Fenestrations, and Permeability, *Circ. Res.*, 2004, **94**(5), 664–670.
31 C. S. Mantzoros, F. Magkos, M. Brinkoetter, E. Sienkiewicz, T. A. Dardeno and S. Y. Kim, *et al.*, Leptin in human physiology and pathophysiology, *Am. J. Physiol.*, 2011, **301**(4), E567–E584.
32 A. Bouloumié, H. C. A. Drexler, M. Lafontan and R. Busse, Leptin, the Product of Ob Gene, Promotes Angiogenesis, *Circ. Res.*, 1998, **83**(10), 1059–1066.
33 J. L. Maymó, A. P. Pérez, Y. Gambino, J. C. Calvo, V. Sánchez-Margalet and C. L. Varone, Review: Leptin gene expression in the placenta – Regulation of a key hormone in

trophoblast proliferation and survival, *Placenta*, 2011, **32**, S146–S153.

34 A. K. Herrera-Vargas, E. García-Rodríguez, M. Olea-Flores, M. A. Mendoza-Catalán, E. Flores-Alfaro and N. Navarro-Tito, Pro-angiogenic activity and vasculogenic mimicry in the tumor microenvironment by leptin in cancer, *Cytokine Growth Factor Rev.*, 2021, **62**, 23–41.

35 P. E. Stürzebecher, S. Kralisch, M. R. Schubert, V. Filipova, A. Hoffmann and F. Oliveira, *et al.*, Leptin treatment has vasculo-protective effects in lipodystrophic mice, *Proc. Natl. Acad. Sci. U. S. A.*, 2022, **119**(40), e2110374119.

36 G. E. Lash, K. Naruse, B. A. Innes, S. C. Robson, R. F. Searle and J. N. Bulmer, Secretion of angiogenic growth factors by villous cytotrophoblast and extravillous trophoblast in early human pregnancy, *Placenta.*, 2010, **31**(6), 545–548.

37 N. Vrachnis, E. Kalampokas, S. Sifakis, N. Vitoratos, T. Kalampokas and D. Botsis, *et al.*, Placental growth factor (PlGF): a key to optimizing fetal growth, *J. Matern.-Fetal Neonat. Med.*, 2013, **26**(10), 995–1002.

38 N. Kosyakova, D. D. Kao, M. Figetakis, F. López-Giráldez, S. Spindler and M. Graham, *et al.*, Differential functional roles of fibroblasts and pericytes in the formation of tissue-engineered microvascular networks in vitro, *npj Regener. Med.*, 2020, **5**(1), 1–12.

39 L. Liu, Y. Jiang and J. J. Steinle, Forskolin regulates retinal endothelial cell permeability through TLR4 actions in vitro, *Mol. Cell. Biochem.*, 2021, **476**(12), 4487–4492.

40 R. Rokhzan, C. C. Ghosh, N. Schaible, J. Notbohm, H. Yoshie and A. J. Ehrlicher, *et al.*, Multiplexed, high-throughput measurements of cell contraction and endothelial barrier function, *Lab. Invest.*, 2019, **99**(1), 138–145.

41 G. P. v. N. Amerongen, R. J. P. Musters, E. C. Eringa, P. Sipkema and V. W. M. van Hinsbergh, Thrombin-induced endothelial barrier disruption in intact microvessels: role of RhoA/Rho kinase-myosin phosphatase axis, *Am. J. Physiol.*, 2008, **294**(5), C1234–C1241.

42 B. Yi, T. Ding, S. Jiang, T. Gong, H. Chopra and O. Sha, *et al.*, Conversion of stem cells from apical papilla into endothelial cells by small molecules and growth factors, *Stem Cell Res. Ther.*, 2021, **12**(1), 266.

43 N. Kandzija, M. Rahbar, G. D. Jones, C. Motta-Mejia, W. Zhang and Y. Couch, *et al.*, Placental capillary pericytes release excess extracellular vesicles under hypoxic conditions inducing a pro-angiogenic profile in term pregnancy, *Biochem. Biophys. Res. Commun.*, 2023, **651**, 20–29.

44 R. S. N. Barreto, P. Romagnolli, A. D. Cereta, L. M. C. Coimbra-Campos, A. Birbrair and M. A. Miglino, Pericytes in the Placenta: Role in Placental Development and Homeostasis, in *Pericyte Biology in Different Organs*, ed. A. Birbrair, Springer International Publishing, Cham, 2019, pp. 125–151, (Advances in Experimental Medicine and Biology), DOI: **10.1007/978-3-030-11093-2_8**.

45 K. Haase, M. R. Gillrie, C. Hajal and R. D. Kamm, Pericytes Contribute to Dysfunction in a Human 3D Model of Placental Microvasculature through VEGF-Ang-Tie2 Signaling, *Adv. Sci.*, 2019, **6**(23), 1900878.

46 M. Cherubini and K. Haase, A Bioengineered Model for Studying Vascular-Pericyte Interactions of the Placenta, in *Cell Migration in Three Dimensions [Internet]*, ed. C. Margadant, Springer US, New York, NY, 2023, pp. 409–423, (Methods in Molecular Biology), DOI: **10.1007/978-1-0716-2887-4_23**.

47 T. H. Wang, H. S. Wang and Y. K. Soong, Paclitaxel-induced cell death, *Cancer*, 2000, **88**(11), 2619–2628.

48 C. Walsh, Deconstructing Vancomycin, *Science*, 1999, **284**(5413), 442–443.

49 A. Gardulf and U. Nicolay, Replacement IgG therapy and self-therapy at home improve the health-related quality of life in patients with primary antibody deficiencies, *Curr. Opin. Allergy Clin. Immunol.*, 2006, **6**(6), 434.

50 A. Gardulf, E. Andersson, M. Lindqvist, S. Hansen and R. Gustafson, Rapid Subcutaneous IgG Replacement Therapy at Home for Pregnant Immunodeficient Women, *J. Clin. Immunol.*, 2001, **21**(2), 150–154.

51 C. Maggen, V. E. R. A. Wolters, E. Cardonick, M. Fumagalli, M. J. Halaska and C. A. R. Lok, *et al.*, Pregnancy and Cancer: the INCIP Project, *Curr. Oncol. Rep.*, 2020, **22**(2), 17.

52 E. Cardonick, A. Bhat, D. Gilmandyar and R. Somer, Maternal and fetal outcomes of taxane chemotherapy in breast and ovarian cancer during pregnancy: case series and review of the literature, *Ann. Oncol.*, 2012, **23**(12), 3016–3023.

53 E. H. Cardonick, A. E. O'Laughlin, S. C. So, L. T. Fleischer and S. Akoto, Paclitaxel use in pregnancy: neonatal follow-up of infants with positive detection of intact paclitaxel and metabolites in meconium at birth, *Eur. J. Pediatr.*, 2022, **181**(4), 1763–1766.

54 S. Girardelli, B. Bonomo, M. Papale, E. di Loreto, E. Grossi, G. Scarfone, E. Rabaiotti, L. Valsecchi, G. Mangili, M. Candiani and F. Peccatori, Weekly paclitaxel for pregnancy associated breast cancer, *Clin. Breast Cancer*, 2024, **24**(3), 199–203.

55 I. A. Nekhayeva, T. N. Nanovskaya, G. D. V. Hankins and M. S. Ahmed, Role of Human Placental Efflux Transporter P-Glycoprotein in the Transfer of Buprenorphine, Levo-α-Acetylmethadol, and Paclitaxel, *Am. J. Perinatol.*, 2006, **23**(7), 423–430.

56 K. V. Calsteren, R. Verbesselt, R. Devlieger, L. De Catte, D. C. Chai and R. Van Bree, *et al.*, Transplacental transfer of paclitaxel, docetaxel, carboplatin, and trastuzumab in a baboon model, *Int. J. Gynecol. Cancer*, 2010, **20**(9), 1456–1464.

57 T. Nanovskaya, S. Patrikeeva, Y. Zhan, V. Fokina, G. D. Hankins and M. S. Ahmed, Transplacental transfer of vancomycin and telavancin, *Am. J. Obstet. Gynecol.*, 2012, **207**(4), 331.e1–331.e6.

58 A. Malek, Role of IgG antibodies in association with placental function and immunologic diseases in human pregnancy, *Expert Rev. Clin. Immunol.*, 2013, **9**(3), 235–249.

59 M. D. Joshi, G. M. Pais, J. Chang, K. Hlukhenka, S. N. Avedissian and A. Gulati, *et al.*, Evaluation of Fetal and Maternal Vancomycin-Induced Kidney Injury during

Pregnancy in a Rat Model, *Antimicrob. Agents Chemother.*, 2019, **63**(10), e00761-19.

60 M. D. Hnat, J. Gainer, R. E. Bawdon and G. D. Wendel, Transplacental passage of vancomycin in the ex vivo human perfusion model, *Infect. Dis. Obstet. Gynecol.*, 2004, **12**(2), 57–61.

61 J. Laiprasert, K. Klein, B. A. Mueller and M. D. Pearlman, Transplacental passage of vancomycin in noninfected term pregnant women, *Obstet. Gynecol.*, 2007, **109**(5), 1105–1110.

62 C. N. Onwuchuruba, C. V. Towers, B. C. Howard, M. D. Hennessy, L. Wolfe and M. S. Brown, Transplacental passage of vancomycin from mother to neonate, *Am. J. Obstet. Gynecol.*, 2014, **210**(4), 352.e1–352.e4.

63 C. V. Towers and B. Weitz, Transplacental passage of vancomycin, *J. Matern.-Fetal Neonat. Med.*, 2018, **31**(8), 1021–1024.

64 R. E. Wessel and S. Dolatshahi, Quantitative mechanistic model reveals key determinants of placental IgG transfer and informs prenatal immunization strategies, *PLoS Comput. Biol.*, 2023, **19**(11), e1011109.

65 T. Clements, T. F. Rice, G. Vamvakas, S. Barnett, M. Barnes, B. Donaldson, C. Jones, B. Kampmann and B. Holder, Update on transplacental transfer of IgG subclasses: impact of maternal and fetal factors, *Front. Immunol.*, 2020, **11**, 1920.

66 Y. Xu, Y. He, S. Momben-Abolfath, D. Vertrees, X. Li and M. G. Norton, *et al.*, Zika Virus Infection and Antibody Neutralization in FcRn Expressing Placenta and Engineered Cell Lines, *Vaccines*, 2022, **10**(12), 2059.

67 A. Malek, R. Sager, A. Zakher and H. Schneider, Transport of immunoglobulin G and its subclasses across the in vitro-perfused human placenta, *Am. J. Obstet. Gynecol.*, 1995, **173**(3), 760–767.

68 R. K. Miller, K. Mace, B. Polliotti, R. DeRita, W. Hall and G. Treacy, Marginal Transfer of ReoPro™ (Abciximab) Compared with Immunoglobulin G (F105), Inulin and Water in the Perfused Human Placenta In Vitro, *Placenta*, 2003, **24**(7), 727–738.

69 S. M. Görisch, K. Richter, M. O. Scheuermann, H. Herrmann and P. Lichter, Diffusion-limited compartmentalization of mammalian cell nuclei assessed by microinjected macromolecules, *Exp. Cell Res.*, 2003, **289**(2), 282–294.

70 T. S. Frost, L. Jiang, R. M. Lynch and Y. Zohar, Permeability of Epithelial/Endothelial Barriers in Transwells and Microfluidic Bilayer Devices, *Micromachines*, 2019, **10**(8), 533.

71 M. Wuhrer, J. C. Stam, F. E. van de Geijn, C. A. M. Koeleman, C. T. Verrips and R. J. E. M. Dolhain, *et al.*, Glycosylation profiling of immunoglobulin G (IgG) subclasses from human serum, *Proteomics*, 2007, **7**(22), 4070–4081.

72 J. Arroyo, R. J. Torry and D. S. Torry, Deferential regulation of placenta growth factor (PlGF)-mediated signal transduction in human primary term trophoblast and endothelial cells, *Placenta*, 2004, **25**(5), 379–386.

73 N. Ricard, R. P. Scott, C. J. Booth, H. Velazquez, N. A. Cilfone and J. L. Baylon, *et al.*, Endothelial ERK1/2 signaling maintains integrity of the quiescent endothelium, *J. Exp. Med.*, 2019, **216**(8), 1874.

74 K. Chau, B. Xu, A. Hennessy and A. Makris, Effect of Placental Growth Factor on Trophoblast–Endothelial Cell Interactions In Vitro, *Reprod. Sci.*, 2020, **27**(6), 1285–1292.

75 K. Rahmouni and W. G. Haynes, Endothelial effects of leptin: Implications in health and diseases, *Curr. Diabetes Rep.*, 2005, **5**(4), 260–266.

76 M. J. Morrison, B. V. Natale, S. Allen, N. Peterson and D. R. C. Natale, Characterizing placental pericytes: Hypoxia and proangiogenic signalling, *Placenta*, 2024, **155**, 1–10.

77 S. E. Harris, K. S. H. Matthews, E. Palaiologou, S. A. Tashev, E. M. Lofthouse and J. Pearson-Farr, *et al.*, Pericytes on placental capillaries in terminal villi preferentially cover endothelial junctions in regions furthest away from the trophoblast, *Placenta*, 2021, **104**, 1–7.

78 E. E. Sharpe, M. A. Rosen and M. D. Rollins, 14-Obstetric Analgesia and Anesthesia, in *Avery's Diseases of the Newborn*, ed. C. A. Gleason and T. Sawyer, Elsevier, Philadelphia, 11th edn, 2024, pp. 147–158.e3, Available from: **https://www.sciencedirect.com/science/article/pii/B9780323828239000143**.

79 N. Utoguchi, G. A. Chandorkar, M. Avery and K. L. Audus, Functional expression of P-glycoprotein in primary cultures of human cytotrophoblasts and BeWo cells, *Reprod. Toxicol.*, 2000, **14**(3), 217–224.

80 G. Castel, D. Meistermann, B. Bretin, J. Firmin, J. Blin and S. Loubersac, *et al.*, Induction of Human Trophoblast Stem Cells from Somatic Cells and Pluripotent Stem Cells, *Cell Rep.*, 2020, **33**(8), 108419.

81 I. Zorzan, R. M. Betto, G. Rossignoli, M. Arboit, A. Drusin and C. Corridori, *et al.*, Chemical conversion of human conventional PSCs to TSCs following transient naive gene activation, *EMBO Rep.*, 2023, **24**(4), e55235.

82 R. M. Karvas and T. W. Theunissen, Generation of 3D Trophoblast Organoids from Human Naïve Pluripotent Stem Cells, in *Embryo Models In Vitro: Methods and Protocols*, ed. M. Zernicka-Goetz and K. Turksen, Springer US, New York, NY, 2024, pp. 85–103, DOI: **10.1007/7651_2023_496**.

83 M. J. Shannon, G. L. McNeill, B. Koksal, J. Baltayeva, J. Wächter and B. Castellana, *et al.*, Single-cell assessment of primary and stem cell-derived human trophoblast organoids as placenta-modeling platforms, *Dev. Cell*, 2024, **59**(6), 776–792.e11.

84 C. Sun, J. L. James and P. Murthi, Three-Dimensional In Vitro Human Placental Organoids from Mononuclear Villous Trophoblasts or Trophoblast Stem Cells to Understand Trophoblast Dysfunction in Fetal Growth Restriction, in *Trophoblasts: Methods and Protocols*, ed. S. Raha, Springer US, New York, NY, 2024, pp. 235–245, DOI: **10.1007/978-1-0716-3495-0_19**.

85 T. Hori, H. Okae, S. Shibata, N. Kobayashi, E. H. Kobayashi and A. Oike, *et al.*, Trophoblast stem cell-based organoid models of the human placental barrier, *Nat. Commun.*, 2024, **15**(1), 962.

86 B. Carrion, I. A. Janson, Y. P. Kong and A. J. Putnam, A Safe and Efficient Method to Retrieve Mesenchymal Stem Cells from Three-Dimensional Fibrin Gels, *Tissue Eng., Part C*, 2014, **20**(3), 252–263.

